Signatures of an energetic charged body streaming in a plasma

Vikram Dharodi [1,*] Atul Kumar [2,†] and Abhijit Sen [1,‡]

[1]*Theoretical Division, Institute for Plasma Research, HBNI, Bhat, Gandhinagar 382428, India*

[2]*Oak Ridge National Laboratory, Oak Ridge, Tennessee 37831, USA*

A charged body moving in a plasma can excite a variety of linear and nonlinear waves in the form of trailing wakes, fore-wake shocks, and precursor solitons. These structures can further interact with the background plasma to create secondary effects that can serve as signatures of the passage of the charged body. Using particle-in-cell simulations, we carry out a basic investigation of the dynamics of a plasma system that is being traversed by an energetic charged body. Using two different shapes of this charged source, namely, an idealized infinite length planar source and a two-dimensional thin rectangular source, we examine the differences in the nature of the excited wave structures and their consequent impact on the background plasma. Our simulations reveal interesting features such as the dependence of the precursor speeds on the total charge on the driving source, local particle trapping, and energization of the trapped particles in various regions along the traversal path leading to the formation of energetic charged beamlets. Our basic findings could find practical applications such as in analyzing the trajectories of charged objects like space debris orbiting in the ionosphere.

I. INTRODUCTION

One of the well-known phenomenon associated with the passage of an object in a neutral fluid is the excitation of trailing waves, more popularly known as wakes or wake fields, behind the object. Apart from these wake fields, it is also possible to excite nonlinear wave structures in the fore-wake region, i.e., ahead of the source when the source speed exceeds a critical value. This well-known hydrodynamic phenomenon has recently been investigated in plasma physics [1–4] and it has been shown that when a charged source moves in an unmagnetized plasma at a speed greater than the ion acoustic speed, a train of nonlinear structures in the form of precursor solitons can arise ahead of the traveling source and move away from it at a faster speed [1]. This nonlinear phenomenon is best understood in terms of a fluid picture. As the object moves through the fluid, it causes an accumulation of matter in front of it causing a rise in the density. Since the object is moving at a supersonic speed, the density perturbations ahead of it cannot linearly disperse because the linear sound velocity is less than the speed of the object. As the density continues to build up in the front, nonlinear effects set in. When the nonlinear steepening is balanced by the dispersive broadening, a soliton can be formed whose velocity is supersonic and can be much faster than the moving object. Hence it moves away from the object. The process is repeated after some time, leading to a chain of solitons. The existence of such precursor

solitons in a plasma has been experimentally confirmed in controlled experiments carried out in a dusty plasma device with the dust fluid made to flow over a charged obstacle at a speed faster than the dust acoustic speed [3]. In principle, such excitations can arise in a magnetized plasma as well in the form of magnetosonic or Alfvenic solitons. Proof-of-principle evidence of the existence of such electromagnetic precursor solitons was provided in an earlier publication [5] using particle-in-cell (PIC) simulations. It was shown that a rigid charged particle source in the form of an infinite planar source could excite these solitons when its velocity exceeded the magnetosonic speed. The simulations also confirmed the existence of electrostatic solitons by turning off the ambient magnetic field and moving the source at a speed faster than the ion acoustic speed. The focus of the earlier study was on delineating the conditions for the excitation of the ion acoustic and magnetosonic precursors in an unmagnetized and magnetized plasma setup, respectively. The precursors were also identified as solitons from their propagation characteristics. The topic of the subsequent interaction of these wave structures with the ambient plasma was not addressed nor was the dependence of the wave properties on the nature of the charged source explored. Our present paper is devoted to an investigation of these questions. We investigate in greater detail the nature of the excited structures using a 2D simulation and study the influence of the source size and strength on the precursors. This is done by comparing the results of propagating a thin rectangular-shaped source with different transverse extents with those obtained for an idealized infinite source. An important difference is found in the propagation characteristics of the two-dimensional (2D) precursors compared to the idealized one-dimensional (1D) ones. While the 1D precursors (solitons) maintain a constant amplitude and width during the course of their propagation, the amplitudes

*vsd005@auburn.edu; present address: Department of Physics, Auburn University, Auburn, Alabama 32849, USA.

†kumara@ornl.gov

‡abhijit@ipr.res.in

of the 2D ones decrease with distance while their widths keep increasing. In both cases, the product of their amplitude with the square of the width remains constant. We also look at the subsequent interactions of the excited waves with the background plasma in various regions along the path of the charged source. These include the wake region, the density depleted region just behind the moving source, and the region ahead of the source where precursor solitary structures propagate. For this, we carry out a detailed study of the temporal evolution of the particle density and energy density in various regions as well as some individual particle kinetics in special regions. For simplicity, we restrict ourselves to excitations created by a positively charged source propagating in an unmagnetized plasma.

Our simulations also show some other interesting differences for the two cases both in the characteristics of the wave structures and their subsequent interaction with the plasma particles. The finite transverse size of the source is seen to introduce a magnetic field component in the excited structures. The propagation speed of the precursors is found to have a direct dependence on the strength of the charge in the source. We also observe significant self-injection of ions in the ion-depleted region immediately behind the charged source. These ions experience energization and focusing effects leading to the formation of beam like structures. Ions are also seen to be trapped between precursor structures and to get energized due to multiple bounces off these structures. The trajectories of these particles are analyzed using particle tagging techniques. The implications and potential applications of these secondary signatures created by the passage of an energetic charged body in the plasma are discussed.

The paper is organized as follows. In Sec. II, we briefly describe the physical model used for our simulations and also give the essential computational details. Our main results are presented in Sec. III with separate subsections devoted to energization due to collective excitations arising from an idealized infinite source (Sec. III A) and a 2D thin rectangular source (an infinite strip source) (Sec. III B). Section IV gives a summary of our results and discusses their relevance and potential for practical applications.

II. SIMULATION MODEL AND DETAILS

We have carried out 2D-3V PIC simulations using the OSIRIS-4.0 code [6–8] for a quasineutral plasma system where the ions are taken to be cold such that the ion thermal velocity $v_{\text{thi}} = 8.85 \times 10^{-5} c$, while the electrons are warm with a thermal velocity $v_{\text{the}} = 0.5c$. At this electron temperature, the ion acoustic sound speed in the medium is [5] $V_{cs} = 0.1c$ ($V_{cs} = \sqrt{k_B T_e/m_i} = v_{\text{the}}/\sqrt{m_i/m_e}$). Furthermore, for simplicity and shorter simulation times, the ion to electron mass ratio m_i/m_e has been taken to be 25. Both these assumptions of a very high ion acoustic speed and unrealistic mass ratio have been taken to speed up the simulations and overcome the constraint of limited available computational facilities. This is not an uncommon practice in PIC simulations [9–11] and is acceptable provided it can be justified for a realistic scenario as will be done later in the paper. We consider a rectangular box of $L_x (= 1000\delta s) \times L_y (= 100\delta s)$ in the $x - y$ plane, where $\delta s (= c/\omega_{pe})$ is the skin depth of the plasma.

L_x and L_y are the system lengths in the x and y directions. Since this is a 2D simulation, by assumption the dimension of the box in the ignored z direction is infinite. The equilibrium plasma density is taken as $n_0 = 3.10 \times 10^{20} \text{cm}^{-3}$. The perturbed density is normalized by the equilibrium plasma density and the electric and magnetic fields are normalized by $m_e c \omega_{pe}/e$. The spatial resolution chosen in the simulation is 20 cells per electron skin depth with 10×10 particles per cell for each species corresponding to a grid size of $\Delta x = 0.05c/\omega_{pe}$ and the temporal resolution is given by the time step $\Delta t = 0.0283\omega_{pe}^{-1}$. In such a plasma system, a positively charged thin (in the x direction) rigid body is made to travel to create linear and nonlinear wave excitations in the plasma. We consider two specific shapes of the charged body: (i) An infinite (in y and z) and finite thickness (in x) plane source whose projection in the $x - y$ plane is a line source and (ii) a finite (in y) thin rectangular strip source. Schematic diagrams corresponding to these two cases are shown in Figs. 1(a) and 1(b), respectively. For all the simulation runs, the charged source is initially positioned at $x = 500\delta s$. In most cases it is made to travel at $V_b = 0.11c$ that is a bit faster than the ion acoustic speed $V_{cs} = 0.1c$. The corresponding Mach number is $M = 1.1$ (where $M = V_b/V_{cs}$). As has been established in molecular dynamics [12] as well as PIC studies [5], precursors happen when the Mach number is greater than one. The speed of the precursor is always faster than the source, implying that as the Mach number increases the precursor speed also increases. Beyond a certain Mach number, one obtains dispersive shock structures [12] or pinned solitons [5]. In our present paper, we do not consider the variation of the precursor propagation as a function of the Mach number but focus on the influence of the shape and size of the source. For simplicity, we have considered a rigid charged source that retains its shape and amount of charge and also does not change its velocity while propagating through the plasma. Real life examples of such a model source can be found, for example, in the form of a charged body representing a space debris object orbiting in the ionosphere.

III. SIMULATION RESULTS AND OBSERVATIONS

The prime objectives of this section are to numerically explore the evolution of wave structures generated using two types of charged sources shown in Fig. 1 and their consequent impact on the background plasma. Both types of sources have constant charge density $\rho_{bm}^c = 1.1$ and the same width $\delta x = 1.02$ (along $\hat{x}$ direction). The source length δy (along $\hat{y}$ direction) is the only parameter that is varied. All the simulations are performed with absorbing boundary conditions in the $\hat{x}$ direction and periodic in the $\hat{y}$ direction for both the particles and the fields.

A. Idealized planar source

We first discuss an infinite length (in y) source case, which excites only longitudinal perturbations in the background plasma. In our 2D simulation (where z is the ignored coordinate), our charge source represents an ideally thin sheet (infinite in the $y - z$ plane) propagating in the x direction. Its projection in the $x - y$ plane is an infinite line. The choice of
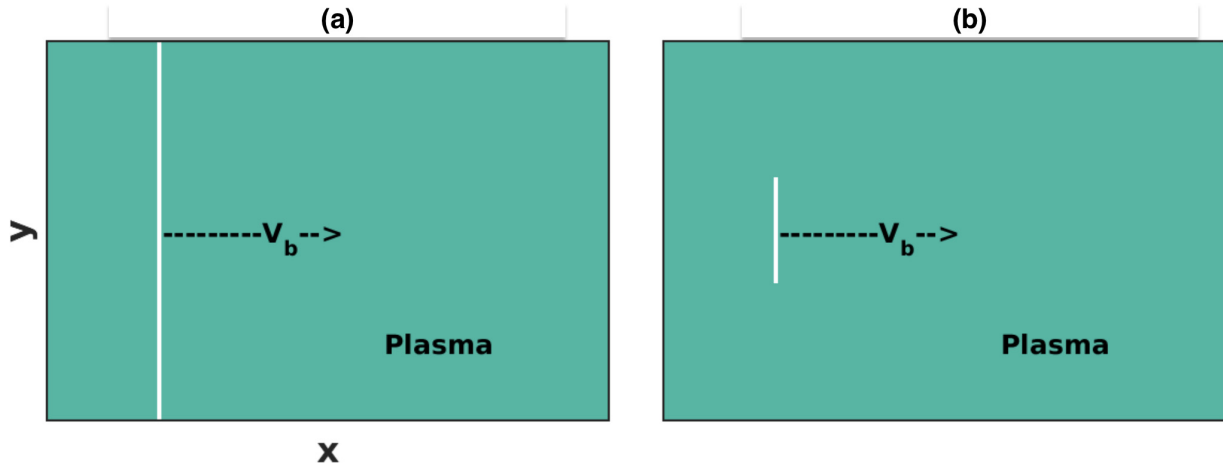
FIG. 1. Schematic diagram (not to scale) of the simulation geometry showing two different-shaped charge sources (a) an infinite (in y and z) and finite thickness (in x) source and (b) an infinite in z, finite (in y) and of finite thickness (in x) source. They move with speed V_b in the positive $\hat{x}$ direction.

this source is to provide a benchmark for studying the effect of a finite size (in the y direction) and to also relate to previous fluid and PIC simulations done for such a shaped source. We have then varied the aspect ratio (length in the y direction, width in the x direction) of the source to study its impact on the precursor excitations. By changing the orientation of the object by 90 degrees, we could also make it a cylinderlike object. Debris objects come in all shapes and sizes, including large planar ones which are called HAMR [13,14] (high area to mass ratio) objects. Our present paper is a representative study of the aspect ratio dependence of a typical source which can be extended in the future to explore other geometrical effects. Understanding this case allows us to determine the impacts of a finite length source. For example, it is of interest to know whether the speed of the perturbations is affected by the transverse dimension of the source and whether it can provide a means of controlling the speed. Figure 2 shows the late-time evolution of the ion charge density $\rho_i^c(x, y)$ due to the passage of a positively charged planar source (vertical

white-solid line) through the plasma. The solid line plots (in black) superposed on these 2D density snapshots represent its 1D profile $\rho_i^c(x)$ as a function of x for the fixed value of $y = 50.03$. This traveling source generates a strong density inhomogeneity in the longitudinal direction.

It is clearly seen that this inhomogeneity is the result of the creation of precursor waves ahead of the source (yellow-colored disturbances), the formation of a region with a depleted number of ions just behind the source (a dark-blue-coloured region), and wake structures following this depressed region (cyan-colored disturbances). Such structures were previously observed in the simulations reported by Kumar and Sen [5] for the case when the ambient magnetic field was taken to be zero. They were obtained to benchmark the code and to also establish connections with previous 1D electrostatic results obtained in fluid simulations. In the present paper, we examine these structures in greater detail to characterize them and to also study their impact on the background plasma.
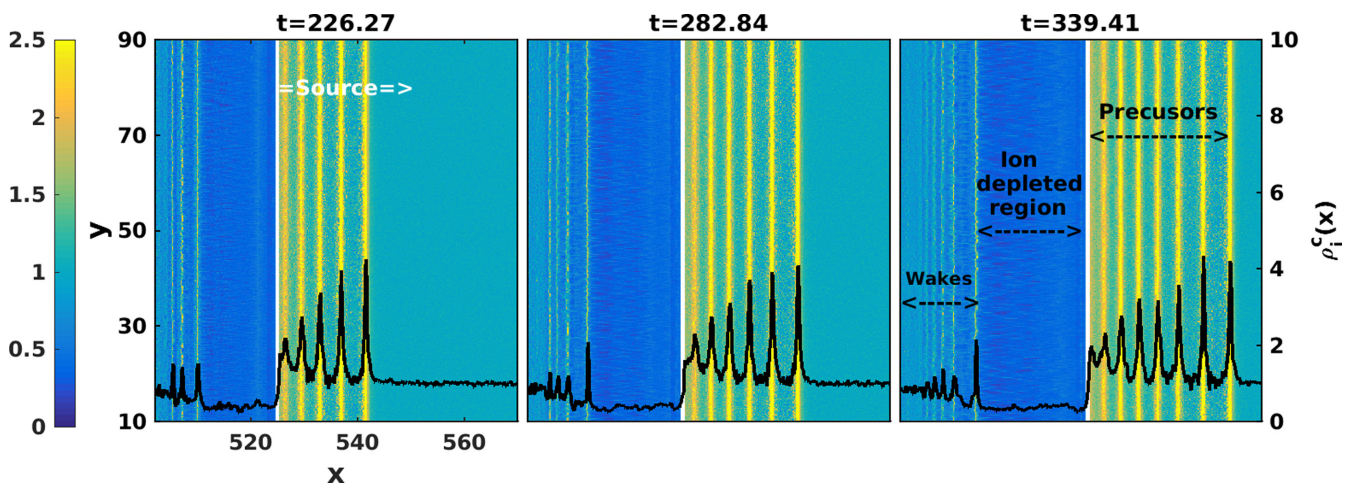

FIG. 2. Time evolution of the ion charge density $\rho_i^c(x, y)$ due to passage of an infinite line source ($\delta x = 1.02$, $\delta y = L_y$). The source creates well-developed trailing wake fields and precursor structures moving ahead of it. The line plots superposed on the snapshots are the profiles of the density $\rho_i^c(x)$ as a function of x for $y = 50.03$ (its scale is given on right y axis).
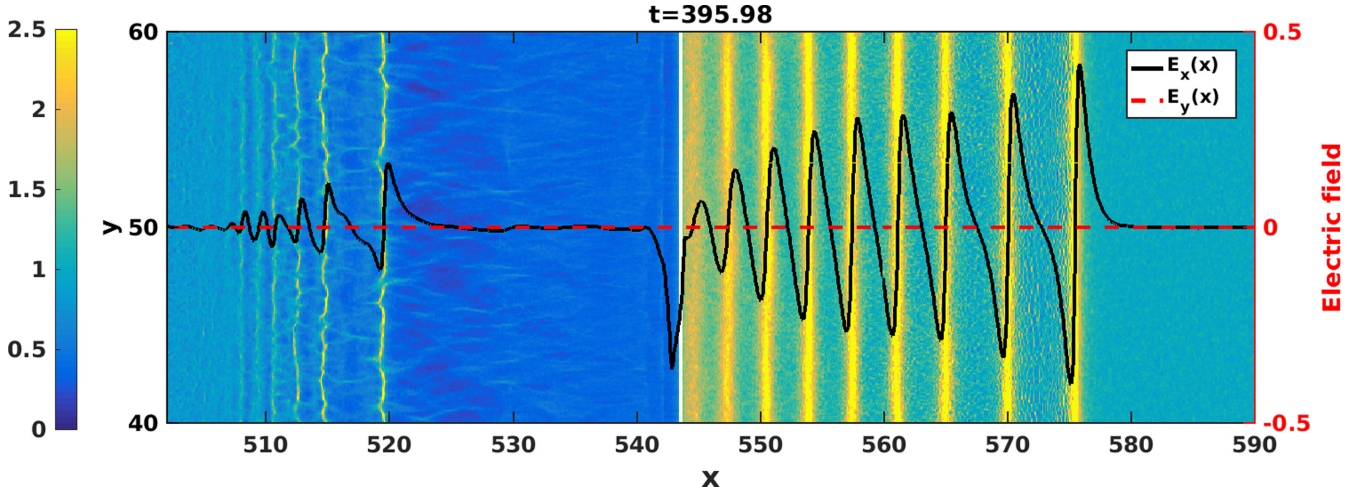
FIG. 3. Spatial variation of electric field components (longitudinal electric field E_x and E_y, normalized to $m_e c \omega_{pe}/e$) with respect to x at a particular instant of time $t = 395.84$. As can be seen, the transverse electric field component E_y is very weak compared to E_x indicating that the one-dimensional precursors are primarily electrostatic in nature.

To establish the basic character of these structures, we first look at the electric field components of these waves. In Fig. 3, we have superposed on the ion charge density color plot, the longitudinal field component, $E_x(x)$, as a black-solid curve, and the transverse component, $E_y(x)$, as a red-dotted curve, at a time $t = 395.98$. For these components of the electric field, the right y axis defines the scale. As can be seen from this figure, the transverse component is extremely weak compared to the longitudinal component indicating that the waves are primarily electrostatic in nature. Furthermore, the density depleted region is nearly free of any electric field and the ion density is uniform in this region. $E_x(x)$ has sharp spikes at either edge of this region that are consistent with the creation of a region of density depression behind the moving source. A careful analysis of Fig. 3 tells us that the electrostatic force for ions in the density depleted region is acting in the forward direction and which can lead to acceleration of any self injected ions in the direction of the source propagation.

We next look at the time evolution of the various structures described above and the changes in the background plasma as a result of their creation. This is best captured in Fig. 4, which shows the temporal evolution of the density and the kinetic energy as a function of x for a fixed value of $y = 50.03$. Since in this simulation case there is uniformity in the y direction, this plot provides a comprehensive picture of the spatiotemporal evolution of wave excitations as well as the background density [Fig. 4(a)] and kinetic energy [Fig. 4(b)] of the system. From Fig. 4(a), we can clearly see that with time the source excites more and more precursor structures ahead of it which move faster than the source. These precursor structures with enhanced ion densities (yellow color) travel along x at a steady pace with a super sonic velocity of $0.2004c$. The velocity can be deduced from the straight line fit (magenta dotted slant line) of $x = 0.2004t + 496.07$ to the trajectory of the precursor. This is consistent with past fluid [1,2] and PIC simulations [5] which have identified these structures as precursor ion acoustic solitons. Figure 4(a) also shows that with the passage of time the region of depressed density keeps on expanding. This can be understood from mass conservation

arguments. Basically as the source generates more and more density enhanced structures (precursor solitons) ahead of it, mass is transferred from the region behind the source to enable this process and hence the depressed region grows in size. Trailing behind the depressed region are the wake structures. Unlike the precursor solitons, these are dispersive structures whose amplitudes die down as a function of the distance behind the depressed region. Far away from the depressed region, the amplitudes are quite small and the waves travel with the group velocity of the linear ion acoustic wave, namely,

$$C_g = \frac{\partial \omega}{\partial k} = \frac{C_s}{\left(1 + k^2 \lambda_d^2\right)^{3/2}}, \tag{1}$$

where k is the wave number and λ_d is the electron Debye length. For our simulation parameters, $\lambda_d \sim 0.5 c/\omega_{pi}$. The wave number $k \sim 1.8 \omega_{pi}/c$, so $k\lambda_d \sim 0.9$. Using (1), this yields a group velocity of $\sim 0.4 C_s$. The velocity of these linear wakes can be deduced from a straight line fit (white dotted slant line) to the green lines shown in the far left portion of Fig. 4(a) and the velocity is found to be $\sim 0.04c \sim 0.4C_s$. The lead portion of the wake, seen as a wave structure with a substantial amplitude, that remains attached to the rear end of the depressed region, travels somewhat faster than the linear wakes. A linear fit (red dotted slant line) to its trajectory yields a velocity of $0.0564c \sim 0.564C_s$. The enhanced velocity can be attributed to finite amplitude effects giving the lead wake structure a nonlinear character.

Finally, in Fig 4(b), we look at the spatiotemporal evolution of the kinetic energy of the system as the source passes through it. The energy of the source and the precursors are predominantly due to their directed velocities. There is no significant heating of the background plasma in the fore-wake region. We also note that the density depressed region shows evidence of background heating of the ions in that region. The weak wake structures do not impact the background energy in any significant manner.
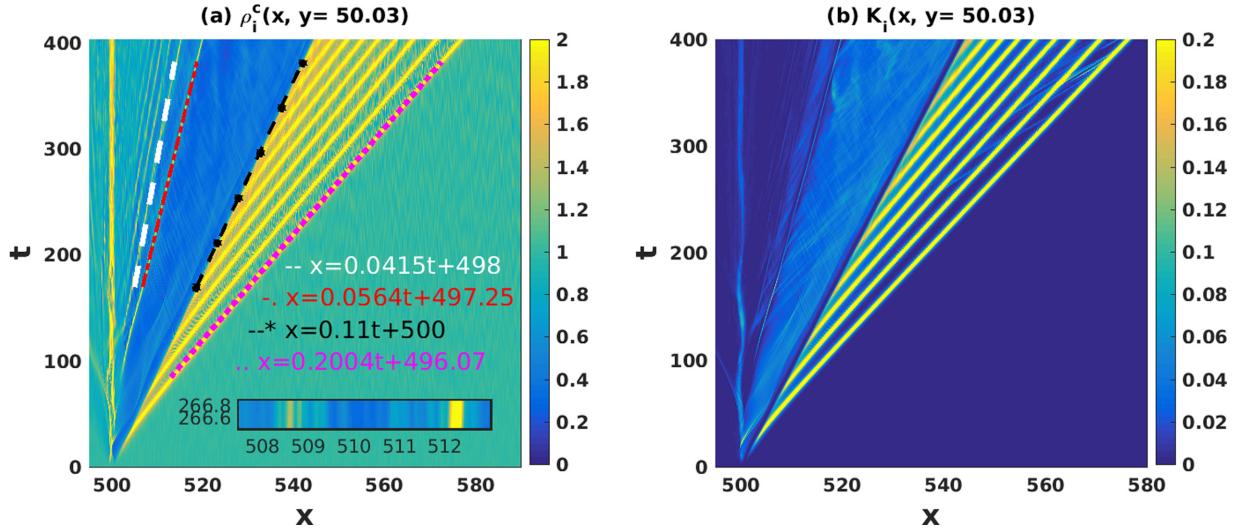
FIG. 4. The temporal evolution of (a) the ion charge density and (b) the kinetic energy at $y = 50.03$ for the 1D simulations. As can be seen from the slopes of the various trajectories in (a), the precursors (shown in yellow) travel faster than the source while the trailing wake structures (green lines) are slower than the source. We also see the density depleted region expanding with time. In (b), we see no evidence of any heating of the background plasma in the fore-wake region and the energy of the source and the precursors are predominantly due to their directed energies.

B. A two-dimensional thin rectangular source

We now turn to the case of a 2D thin rectangular source (a thin strip source) moving through the plasma as shown schematically in Fig. 1(b). In contrast to the infinite planar case described in the previous section, the source now has a finite transverse dimension δy along the $\hat{y}$ direction. The finite transverse dimension has a profound influence on the nature of the induced excitations as well as on the interactions of these structures with the background plasma.

A quick comparative overview of the influence of the transverse length on the nature of the wave excitations is shown in Figs. 5(a)–5(c), where snapshots of the background ion charge density $\rho_i^c(x, y)$ are presented at $t = 282.84$ for simulations with $\delta y = 100, 14$, and 8, respectively. All other parameters are kept the same for these runs. The vertical white line shows the location of the source. One of the first differences one notices is in the shapes of the precursors which now bend back at the tips to give rise to a crescentlike structure. The bending becomes more pronounced as the transverse length of the source diminishes—a distinctly hydrodynamic phenomenon as the movement of the plasma flow around the source tries to attain a streamlined form. Note that this is different from a hydrodynamic bow wave that is normally formed around a ship's prow [15]. The hydrodynamic bow wave remains attached to the moving source quite unlike our precursor structures which separate from the source and move away from it at a faster

TABLE I. Constancy of aL^2 for the precursor solitons of Fig. 6.

Soliton	t $\left(\omega_{pe}^{-1}\right)$	a $(\delta n_i / n_0)$	L (c/ω_{pe})	aL^2
Left	339.41	0.7311	0.8	0.4679
Middle	339.41	0.5665	0.93	0.4795
Right	339.41	0.4771	1.0	0.4771

speed. We also notice a slight decrease in the speed of the precursor with a reduction in the transverse size of the source. This can be discerned (as marked in Fig. 5) from the distances traveled by the peaks of the leading precursors for the different cases within the same fixed period of time. The physical reason for this reduction in speed can be attributed to the decrease in the charge strength of the source as the transverse length decreases. The decrease in the strength of the source is also responsible for the fewer number of precursors generated for the $\delta y = 8$ case compared to the others and the decrease in the number of wakes. One also notices a reduction in the size of the ion depleted region—a geometric consequence of the decrease in the transverse source length. This region now displays both longitudinal and transverse inhomogeneities in the density.

We next take a closer look at the $\delta y = 8$ case to discuss the propagation characteristics of the precursor and also the dynamics of the background particles in the various regions. To characterize the nature of their propagation, an enlarged image of the $\delta y = 8$ case has been shown in Fig. 5(d) at $t = 339.41$. In this figure, the superposed line plots again give the density profiles of the precursors. As can be seen, the amplitudes of the precursors diminish with distance while their widths keep increasing. The values of these quantities are given in Table I, which shows that the product of their amplitudes a with the square of their widths L^2 remains constant. This is a characteristic property of a 2D soliton [16–18]. This is in contrast to 1D solitons, which are known to keep their amplitudes and widths constant during the course of their propagation.

We next look at the impact of the source-induced wave structures on the background plasma. A consolidated impression can be obtained from an examination of Figs. 6 and 7. Figure 6(a) shows a series of snapshots of the ion charge density $\rho_i^c(x, y)$ taken at various times, while Fig. 6(b)
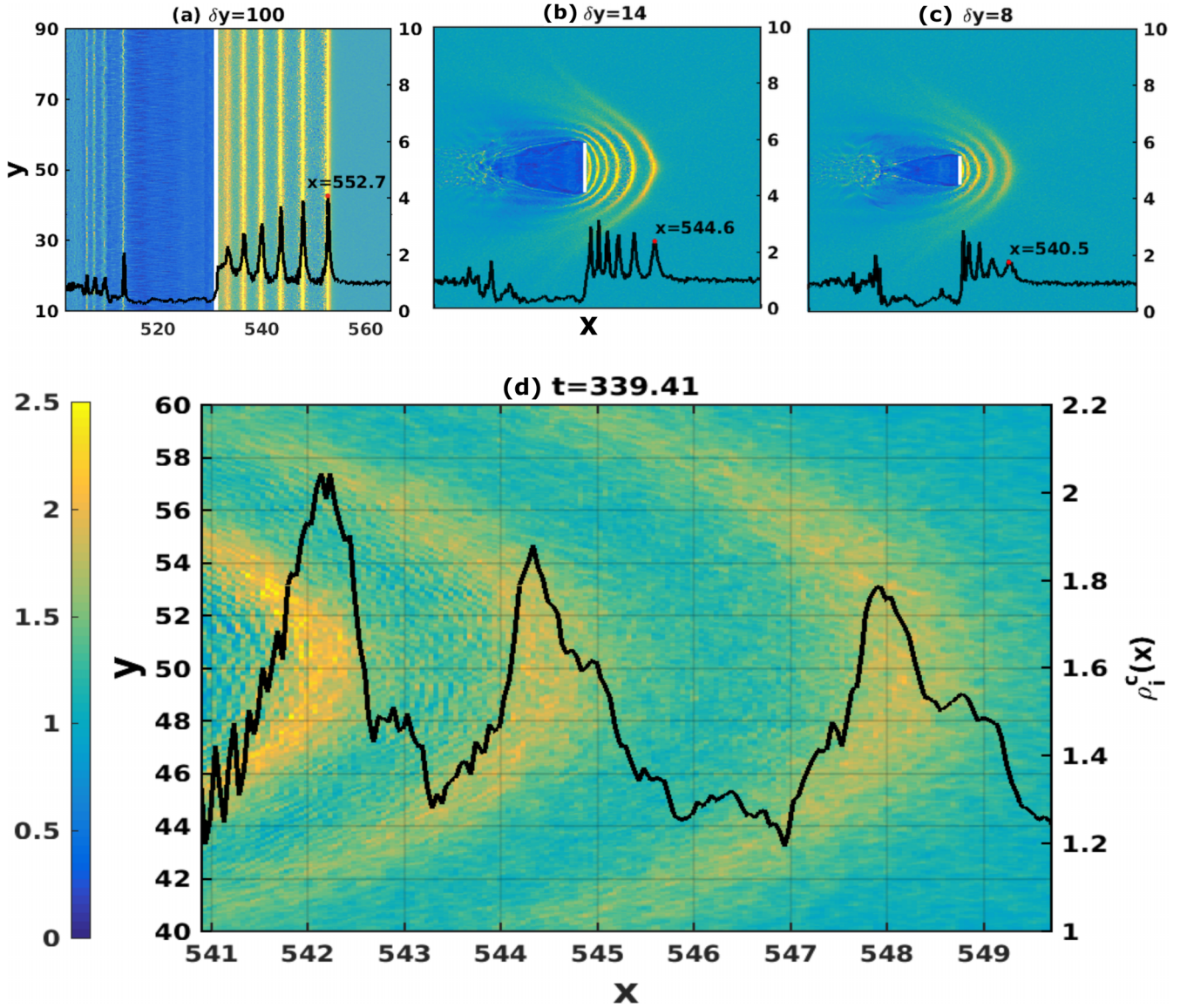
FIG. 5. Snapshots of the background ion charge density $\rho_i^c(x, y = 50.03)$ at $t = 282.84$ for charged sources of three different transverse lengths $\delta y = 100$, 14, and 8 at $t = 282.84$ to highlight the influence of the transverse dimension of the source on the shape of the precursor soliton. It is seen that with a decrease in the transverse size of the source, the precursor soliton tips keep bending more and more backward to form sharper crescent shapes. The vertical white line shows the location of the source. In (d), we present a zoomed view of (c). It is seen that the amplitudes of the precursors diminish with distance while their widths keep increasing. Numerical values of these quantities are given in Table I, which shows that the product of their amplitudes a with the square of their widths L^2 remains constant. This is a characteristic property of a two-dimensional soliton. Note: The color bar is common for all the subplots (a)–(d).

displays the corresponding snapshots of the ion kinetic energy $K_i(x, y)$.

One observes a number of interesting features in Fig. 6, both in the density depletion region and in the precursor region. As the source propagates, the depletion region starts filling up with particles that are self-injected from the background plasma. This is evident at $t = 113.14$ and beyond, through the appearance of an increase in the ion population [shown in light blue in the plots of $\rho_i^c(x, y)$] in the evacuated region that was originally in dark blue. In Fig. 6(b), one also sees evidence of the energization of these self-injected ions inside the evacuated region and a focusing effect leading to the formation of a beamlike structure. The injected ions enter

through the tail region of the depleted region, where they are swept in from the region ahead of the source by the action of the curving precursor waves. Such a self-injection is not seen in the planar case since the ions ahead of the source cannot go around it due to the infinite extent of the source. Another interesting feature, distinctly visible in the rightmost plot of Fig. 6(b) is the trapping of particles between two precursors. These particles get energized by bouncing back and forth between the two wavefronts.

This is brought out more clearly in Figs. 7(a)–7(c), where the progress of four tagged particles p_1 (✳), p_2 (●), p_3 (◆), and p_4 (■) are monitored. At $t = 362.04$, these four particles are tagged at different locations of the simulation domain: p_2
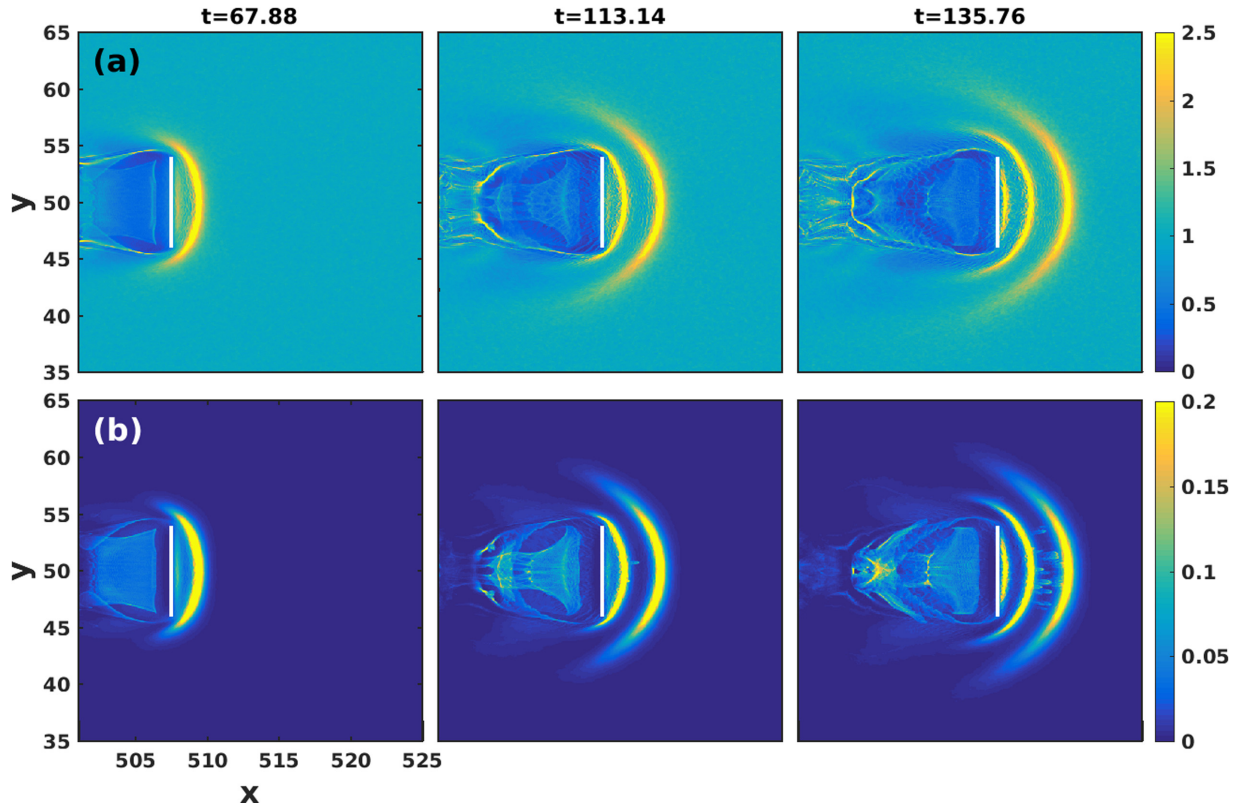
FIG. 6. The evolution of (a) the ion charge density $\rho_i^c(x, y)$ at various times while (b) displays the corresponding ion kinetic energy $K_i(x, y)$. Some self-injection of ions is evident in the bubble regions in (a) as light blue regions showing ion accumulation in the otherwise dark blue ion evacuated region of the bubble. In (b), the yellow streaks between the two leading precursors indicate formation of energetic beamlets.
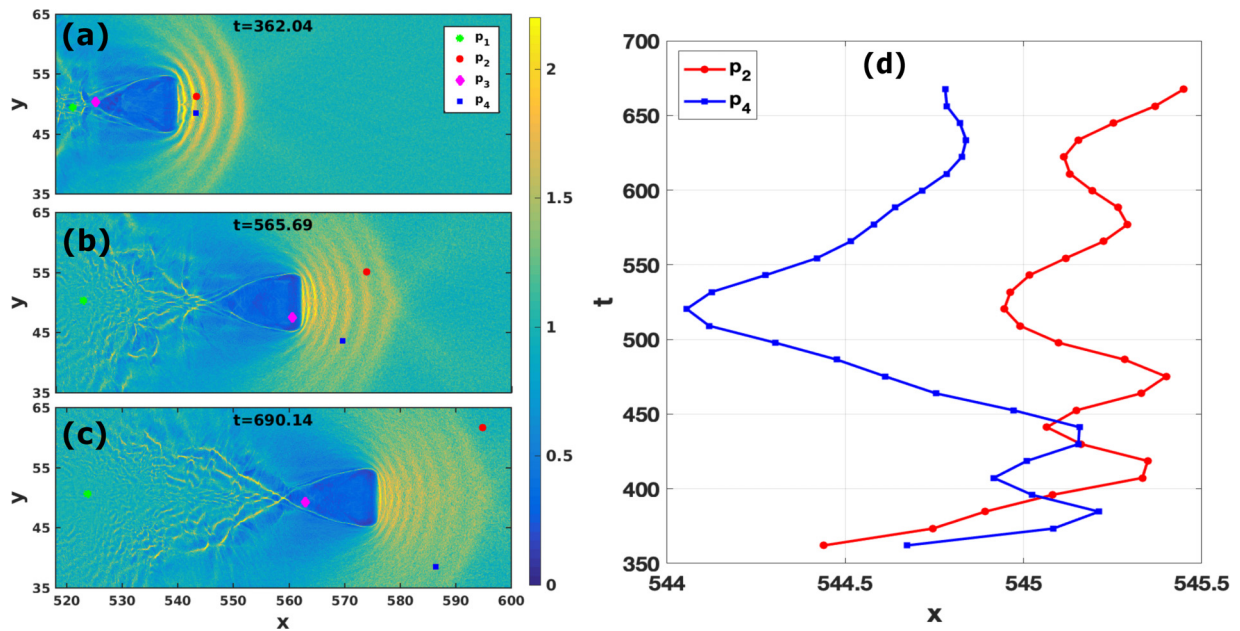

FIG. 7. (a)–(c) Tagging and tracking. p_1 (✳), p_2 (●), p_3 (◆), and p_4 (■) are the four tagged particles. Initially, p_2 and p_4 are the particles tagged between the two precursors and p_1 and p_3 are tagged at the back end of the bubble. Out of these four particles, one particle p_3 gets accelerated in the ion bubble or wake-field region and particle p_4 gets energized and eventually gets untrapped. (d) The bouncing motion of the trapped particles p_2 and p_4 is made evident from their trajectories in the x direction.
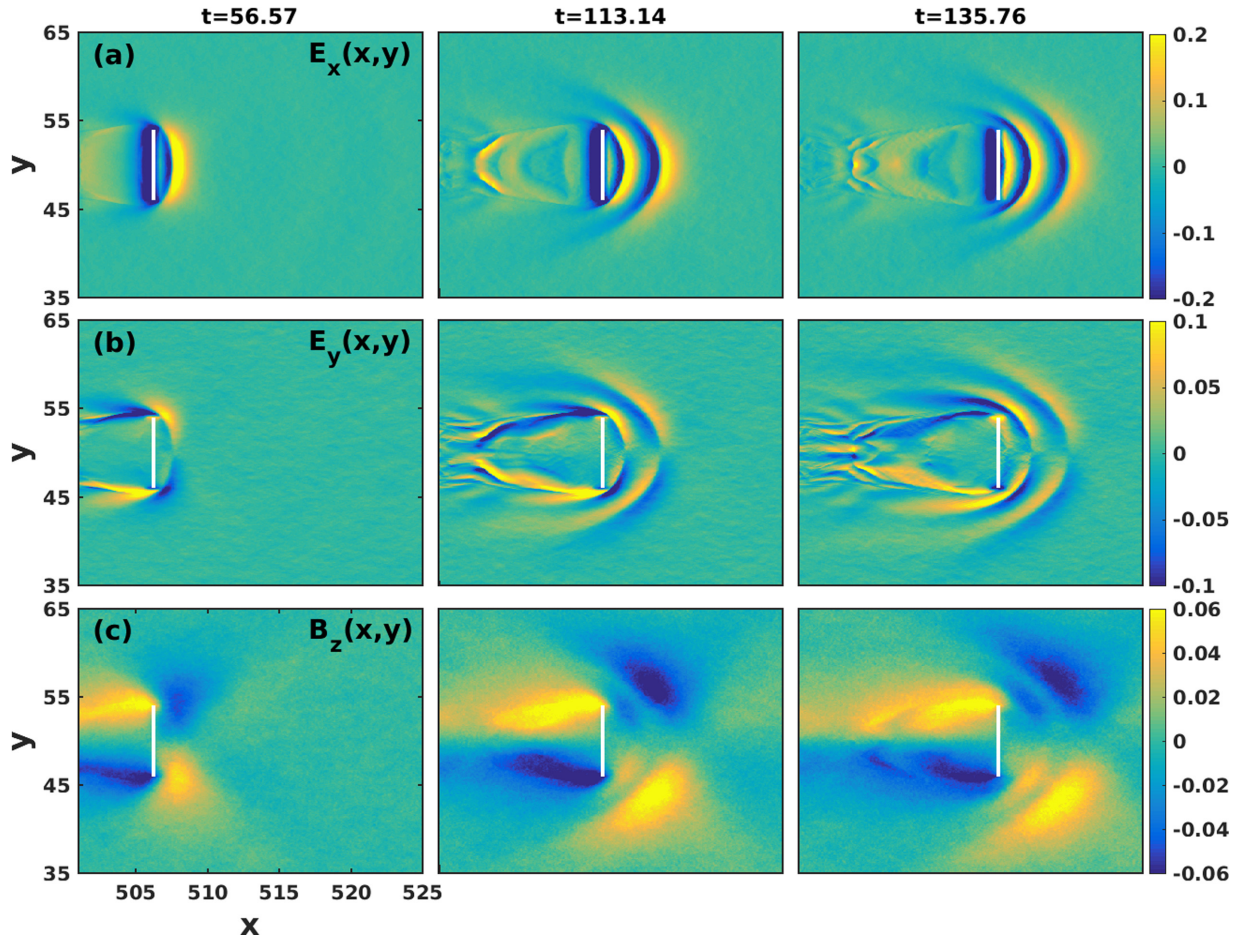
FIG. 8. The field components (normalized to $m_e c \omega_{pe}/e$) of the excited waves: (a) $E_x(x, y)$, (b) $E_y(x, y)$, and (c) $B_z(x, y)$. The presence of E_y and also a finite magnetic field component B_z show that these near-field wave components are no longer purely electrostatic, as was seen for the infinite planar charge source case, but have a non-negligible electromagnetic component. This is another distinctive feature arising from the finite transverse dimension of the charged source.

and p_4 are the particles tagged between the two precursors, whereas p_1 and p_3 are tagged at the back end of the depleted region. The time evolution of these particles shown in Figs. 7(a)–7(c) explains their overall dynamics. The particles p_2 (●) and p_4 (■) originally tagged between the two precursor structures get entrapped. As time progresses, they bounce back and forth between those two wavefronts, get energized, and eventually in this process, they get untrapped. The trapping of these two particles between two precursor wavefronts are shown more clearly in Fig. 7(d), where the positions of the particles in the x direction are plotted as a function of time. As can be seen, the particle orbit exhibits a back-and-forth motion in x, indicating a trapping phenomenon. Eventually, as these particles gain more energy they are pushed ahead of the precursors in the forward direction. These particles then travel faster than the precursors. In certain cases, groups of ions undergo such an acceleration and emerge in the form of thin beamlets. Furthermore, the particle $p3$ (◆) which is placed exactly at the back end of the depleted region sees a huge electrostatic force acting in the forward direction. This force pulls this particle inside the region and accelerates it in the forward direction. The particle $p1$ (✳) which was placed

slightly away from the back end of the region does not suffer any kind of acceleration.

Finally, we discuss one more marked difference between the 1D case and the present 2D simulation. This is in the nature of the wave excitations. Figure 8 shows the field components of the excited waves.

Unlike the 1D case, we now have both E_x and E_y and also a finite magnetic field component B_z. In other words, these near-field wave components are no longer purely (or predominantly) electrostatic, as was seen for the infinite planar charge source case, but have a non-negligible magnetic component. This is seen in all regions of the wave propagation—precursors, depleted region, and the wake region. It is important to point out that the wave excitations (wakes as well as precursors) in our simulations are due to a charged source that is *moving uniformly* in the plasma. This has to be distinguished from radiation emerging from an accelerating charge or an oscillating charge (as in an antenna). Thus, in our case the near-field measurements are the relevant ones, unlike those carried out for standard antenna outputs. We identify the presence of such a magnetic component as one more signature of a finite-sized charged object moving in

the plasma. Similar signatures have been noted earlier in other contexts in the literature and our observations are in line with those [19–21].

IV. DISCUSSION

In this paper, we have investigated the nature of linear and nonlinear collective excitations arising from the passage of an energetic charged body in a plasma. Furthermore, we have examined the interaction of these waves with the ambient plasma. These excitations include both trailing wakes and fore-wake structures. Such structures are likely to arise whenever the source speed exceeds the phase speeds of some of the basic collective modes of the system. In the present paper, we have restricted ourselves to an unmagnetized plasma and considered cases where the source speed exceeds the ion acoustic speed of the plasma. We have considered a positively charged source, but similar results can also be obtained for a negatively charged source as was remarked in Ref. [5]. We have then varied the transverse dimension of the source to create different configurations of the source ranging from an infinite planar source to 2D thin rectangular strips of different transverse sizes. We find that the shape and size of the source have a profound influence on the nature of the precursor waves. One significant difference between the 1D and 2D precursor solitons is in the nature of their evolution in space. While a 1D precursor maintains a constant amplitude and width during its propagation, the amplitude of the 2D precursor decreases with distance and its width increases. In both cases, the product of the amplitude and square of the width remains a constant. This is in accord with theoretical predictions of 1D and 2D solitons [16,17]. Furthermore, it is seen that reducing the transverse dimension of the source causes a slowing down of the precursor and also bends it at the edges to create a crescentlike structure. Since the charge density of the source is kept constant, reducing the transverse length reduces the area of the source and hence the amount of charge on it. The reduction of the charge and hence the strength of the source leads to a reduction of the speed of the precursor and also to the number of precursors created in a given amount of time. The bending of the precursors is a geometric effect directly related to the shape of the source influencing the flow of the plasma around it. The finite transverse size of the source also introduces a modification in the field characteristics of the precursor and other source induced excitations in that they are no longer purely electrostatic but have a magnetic component to it. Such a modification arising from finite-size effects had been predicted theoretically [19–21] and observed experimentally [22] in other contexts.

With respect to the interaction of these waves with the ambient plasma, we observe interesting features such as the formation of a density-depleted region and the trapping of ions and their subsequent acceleration inside that region. Our particle-tagging studies demonstrate this very clearly. The formation of beamlets provides a distinct signature of such an acceleration and focusing within the depleted region. The existence of the precursors provides an additional mechanism for particle trapping and energization of ions. The basic mechanism is akin to Fermi acceleration due to repeated

bouncing off these intense field structures. We also see evidence of beamlet formation in the fore-wake region arising due to particle trapping and acceleration in regions between precursors.

We now discuss some of the assumptions and simplifications made in our simulations and their impact on our results. Our present simulations are restricted to excitation of ion acoustic wakes and precursors in an unmagnetized plasma. Many basic laboratory plasmas, such as those created in glow discharge devices, Q machines [23], etc., are unmagnetized and our results can be easily tested in such experiments. Furthermore, as is well-known [24], both linear and nonlinear ion acoustic waves can be excited in unmagnetized as well as magnetized plasmas (in the direction along the magnetic field). It should also be mentioned that magnetization is best quantified in terms of the parameter $\beta = \frac{nk_B T}{B^2/2\mu_0}$, the ratio of the plasma pressure to the magnetic pressure. In a high beta plasma (low magnetic field and high density high temperature plasma), the electron and ion orbits are not much affected by the magnetic field and the plasma can be considered to be unmagnetized and the propagation properties of low-frequency electrostatic waves, like ion acoustic waves, are not influenced by the magnetic field. High β plasmas can occur in many astrophysical objects as well as in the ionosphere [25,26] [e.g., in the geosynchronous Earth orbit (GEO) region], and hence our findings can be usefully applied to such plasmas. In our simulations, we have also made the standard assumption of treating the ions to be cold (i.e., $T_e \gg T_i$) since the propagation characteristics of the ion acoustic wave are primarily governed by the electron pressure and the ion inertia [24].

A major simplification has been that of taking an unrealistic ion to electron mass ratio of 25 as well as a very high value of the electron temperature. As mentioned above, this has been done to reduce the simulation time and is justified, provided one can show the scaling of the results to realistic scenarios. In our case, the above-mentioned quantities determine the ion acoustic speed and concomitantly the speed of the source for a fixed Mach number. The ion acoustic speed determines how rapidly the precursors separate from the source and from each other since their speeds are supersonic. A low ion acoustic speed (and hence also a low source speed) would imply a longer period for a reasonable separation of the precursors and one would have to carry out a longer simulation run. The timescale is linear with the ion acoustic speed. We have confirmed this by carrying out a run in which the ion acoustic speed was lowered by a factor of 2 by increasing the mass ratio by a factor of 4. The source speed was accordingly lowered by a factor of 2 to maintain the same Mach number. A comparison of the two runs is shown in Fig. 9. As can be seen, the bottom panel recreates exactly the phenomenon observed in the top panel but at a time that is two times later. Thus, our main findings regarding the occurrence and nature of precursors remains the same for the two different choices of the mass ratio and can be easily scaled up to realistic physical parameters.

Another major simplification pertains to the source which is assumed to maintain its rigidity and also not lose any energy or charge during its propagation. Our source model is motivated by and based on real life examples like an orbiting
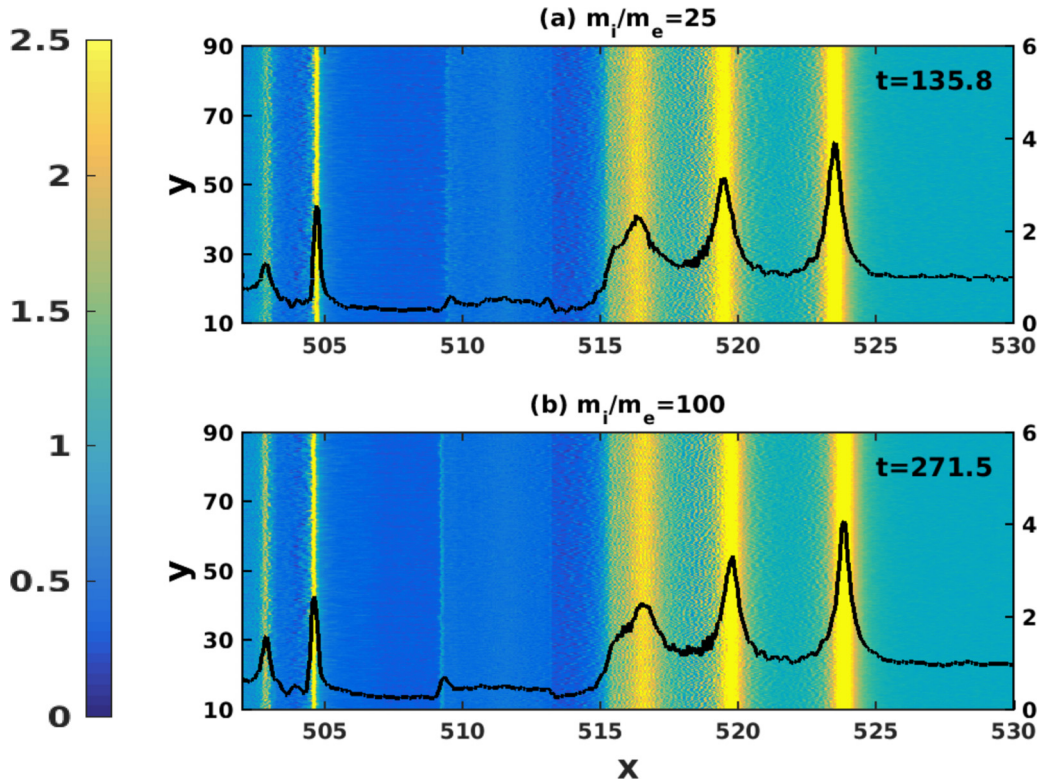
FIG. 9. A comparison of the precursor excitations by a line source for two different values of the mass ratio, namely, 25 and 100, while maintaining the same Mach number of 1.1. As can be seen, the basic phenomenon of precursor excitation and the nature of the precursor remains the same in both cases with a time delay that is linearly proportional to the ion acoustic speeds for the two cases. For the higher mass ratio of 100, the phenomenon occurs at twice the time period compared to that of 25.

space debris object. Such an object gets quickly charged by the ionospheric plasma and the amount of charge does not change apart from small fluctuations due to the dynamic nature of the plasma charging process. The object also possesses a large kinetic energy due to its large mass and its high orbital velocity. Collisional drag effects are negligible in the orbital regions where the debris objects are abundant [namely, in the low Earth orbit (LEO) and GEO] and the drag induced orbital decay times range from ~25 years at an orbit height of 900 kms to hundreds of years at higher altitudes [27]. Thus it is reasonable to assume a constant orbital velocity for them over the time scales associated with the wave excitations.

To summarize, our present simulations reveal a number of interesting features associated with the excitation of wake and fore-wake structures by a streaming charged object in a plasma. The characteristics of these linear and nonlinear excitations, that are functions of the size and shape of the source, serve as primary signatures of the passage of the charged object in the plasma. Our simulations further show that the subsequent interaction of these structures with the background plasma can create secondary signatures in the form of local particle trapping and particle energization or focusing to create beamlet structures. Experimental detection of these signatures can be helpful in tracing the orbital history of the streaming charged source and can also provide insights into the complex wave-particle dynamics of the (fore) wake-field interactions with the plasma. Although our simulations use an idealized model of the charged source, our results could be useful in certain practical applications where the model assumptions are justified. As discussed above, our model source provides a realistic description of a charged debris object and hence the detection of these plasma signatures can be helpful in the detection of such debris objects in the LEO and GEO orbital regions.

Finally, we would like to add that our present studies, carried out for unmagnetized plasmas, can be easily extended to magnetized plasmas where in the past we have demonstrated the existence of magnetosonic precursors [5]. Such an investigation is presently in progress and is also being extended to three-dimensional simulations to provide a more realistic assessment for practical applications. These results will be reported separately.

[1] A. Sen, S. Tiwari, S. Mishra, and P. Kaw, Nonlinear wave excitations by orbiting charged space debris objects, Adv. Space Res. **56**, 429 (2015).

[2] S. K. Tiwari and A. Sen, Wakes and precursor soliton excitations by a moving charged object in a plasma, Phys. Plasmas **23**, 022301 (2016).

[3] S. Jaiswal, P. Bandyopadhyay, and A. Sen, Experimental observation of precursor solitons in a flowing complex plasma, Phys. Rev. E **93**, 041201 (2016).

[4] G. Arora, P. Bandyopadhyay, M. G. Hariprasad, and A. Sen, Effect of size and shape of a moving charged object on the propagation characteristics of precursor solitons, Phys. Plasmas **26**, 093701 (2019).

[5] A. Kumar and A. Sen, Precursor magneto-sonic solitons in a plasma from a moving charge bunch, New J. Phys. **22**, 073057 (2020).

[6] R. G. Hemker, Ph.D. thesis, Particle-in-cell modeling of plasma-based accelerators in two and three dimensions, University of California, Los Angeles, 2000.

[7] R. A. Fonseca, L. O. Silva, F. S. Tsung, V. K. Decyk, W. Lu, C. Ren, W. B. Mori, S. Deng, S. Lee, T. Katsouleas *et al.*, Osiris: A three-dimensional, fully relativistic particle in cell code for modeling plasma based accelerators, *International Conference on Computational Science* (Springer, Heidelberg, 2002), pp. 342–351.

[8] R. A. Fonseca, S. F. Martins, L. O. Silva, J. W. Tonge, F. S. Tsung, and W. B. Mori, One-to-one direct modeling of experiments and astrophysical scenarios: Pushing the envelope on kinetic plasma simulations, Plasma Phys. Controlled Fusion **50**, 124034 (2008).

[9] R. A. Treumann and W. Baumjohann, Collisionless magnetic reconnection in space plasmas, Frontiers Phys. **1**, 31 (2013).

[10] A. Mishchenko, A. Biancalani, A. Bottino, T. Hayward-Schneider, Ph. Lauber, E. Lanti, L. Villard, R. Kleiber, A. Koenies, and M. Borchardt, Numerics and computation in gyrokinetic simulations of electromagnetic turbulence with global particle-in-cell codes, Plasma Phys. Controlled Fusion **63**, 084007 (2021).

[11] G. R. Werner, S. Robertson, T. G. Jenkins, A. M. Chap, and J. R. Cary, Accelerated steady-state electrostatic particle-in-cell simulation of Langmuir probes, Phys. Plasmas **29**, 013502 (2022).

[12] S. K. Tiwari and A. Sen, Fore-wake excitations from moving charged objects in a complex plasma, Phys. Plasmas **23**, 100705 (2016).

[13] T. Schildknecht, R. Musci, and T. Flohrer, Properties of the high area-to-mass ratio space debris population at high altitudes, Adv. Space Res. **41**, 1039 (2008).

[14] C. Früh, T. M. Kelecy, and M. K. Jah, Coupled orbit-attitude dynamics of high area-to-mass ratio (HAMR) objects: Influence of solar radiation pressure, earth's shadow and the visibility in light curves, Celest. Mech. Dyn. Astr. **117**, 385 (2013).

[15] H. Lamb, *Hydrodynamics* (Cambridge University Press, Cambridge, UK, 1993).

[16] S. Maxon and J. Viecelli, Cylindrical solitons, Phys. Fluids **17**, 1614 (1974).

[17] S. Maxon and J. Viecelli, Spherical Solitons, Phys. Rev. Lett. **32**, 4 (1974).

[18] T. Romesser and N. Hershkowitz, Experimental observations of the dimensionless scaling of planar and cylindrical ion acoustic solitons, Phys. Lett. A **53**, 180 (1975).

[19] S. V. Yadavalli, Electromagnetic wake of a charged-particle pulse in a plasma, Phys. Fluids **8**, 956 (1965).

[20] R. K. Bera, D. Mandal, A. Das, and S. Sengupta, Effect of transverse beam size on the wakefields and driver beam dynamics in plasma wakefield acceleration schemes, AIP Adv. **10**, 025203 (2020).

[21] A. Das, A. Kumar, C. Shukla, R. K. Bera, D. Verma, D. Mandal, A. Vashishta, B. Patel, Y. Hayashi, K. A. Tanaka *et al.*, Boundary driven unconventional mechanism of macroscopic magnetic field generation in beam-plasma interaction, Phys. Rev. Res. **2**, 033405 (2020).

[22] G. Chatterjee, K. M. Schoeffler, P. K. Singh, A. Adak, A. D. Lad, S. Sengupta, P. Kaw, L. O. Silva, A. Das, and G. R. Kumar, Magnetic turbulence in a table-top laser-plasma relevant to astrophysical scenarios, Nat. Commun. **8**, 1 (2017).

[23] N. Hershkowitz and Y.-C. G. Kim, Probing plasmas with ion acoustic waves, Plasma Sources Sci. Technol. **18**, 014018 (2009).

[24] R. Fitzpatrick, *Plasma Physics: An Introduction* (CRC Press, Boca Raton, 2022).

[25] A. Gurevich, *Nonlinear Phenomena in the Ionosphere* (Springer Science & Business Media, 1978), Vol. 10.

[26] M. C. Kelley, *The Earth's Ionosphere: Plasma Physics and Electrodynamics* (Academic Press, Amsterdam, 2009).

[27] G. Ganguli, C. Crabtree, L. Rudakov, and S. Chappie, Active debris removal by micron-scale dust injection, *2012 IEEE Aerospace Conference* (IEEE Aerospace Conference, Big Sky, MT, USA, 2012), pp. 1–9.

[28] http://energy.gov/downloads/doe-public-access-plan.